

## EXPERIMENTAL AND NUMERICAL COMPARISON OF THERMODYNAMIC PERFORMANCES OF NEW AND OLD GENERATION REFRIGERANTS IN THE SAME COOLING SYSTEM

by

**Mehmet DAS<sup>a\*</sup> and Oguzhan PEKTEZEL<sup>b</sup>**

<sup>a</sup>Engineering Faculty, Mechatronics Engineering Department, Firat University, Elazig, Turkey

<sup>b</sup>Mechanical Engineering Department, Tokat Gaziosmanpasa University, Tokat, Turkey

Original scientific paper

<https://doi.org/10.2298/TSCI220205069D>

*The use of new generation low GWP refrigerants in cooling systems is becoming increasingly common due to thermal performance and less environmental impact. In this study, the thermal performance of the new generation R290 refrigerant and the old generation R404A refrigerant in the same cooling system were investigated experimentally and numerically. The thermal performance values of both gases were compared, provided that the temperature of the cold room cooled by the vapor compression cooling system drops to 0 °C. -5 °C, 0 °C, 5 °C evaporator temperatures and 25 °C, 30 °C, 35 °C condenser temperatures were used as operating parameters. The experimental results revealed that the highest COP values in the system for R290 and R404A were 4.68 and 3.94, respectively. An average of 9.38% increase in cooling capacity was detected with R290 compared to R404A refrigerant. In the numerical analysis part of the study, the evaporator surface temperature and air velocity distributions of both refrigerants in the cold room were shown numerically by using ANSYS FLUENT 19.1. As a result of the study, it was stated that R290 had higher thermal performance than R404A, according to both experimental and numerical analysis results.*

*Key words: cold room, R290, thermal performance, COP, CFD analysis*

### Introduction

Refrigeration systems are very important because of their various application areas extending from medicine sector and human being's thermal comfort to the industrial processes like food storage [1]. Fast increase in human population in the world caused a rise in refrigeration and air conditioning demand. For instance, 1% of the population in China had air conditioner in 1990 while 100% had by 2009 [2]. Refrigeration systems are among the main causes of energy consumption in the world, and 30% of the world's energy production is spent on these systems [3].

The Paris Agreement in 2015 and the Kigali Amendment of the Montreal Protocol in 2016 highlighted the significant reductions of hydrofluorocarbons (HFC) [4]. For this reason, utilizing of new-generation refrigerants is necessary and urgent. Hydrocarbons (HC) are

---

\*Corresponding authors, e-mail: m.das@firat.edu.tr, oguzhan.pektezel@gop.edu.tr

natural and environmentally friendly refrigerants. They have zero ozone depletion potential (ODP) and low GWP compared to HFC. Refrigerants such as R290 (propane), R600a (isobutane), and R1270 (propylene) can be classified in HC group. The high flammability values of HC are known to be the biggest disadvantage of this fluid type, and this leads to the limitation of refrigerant charge amounts [5].

Although there are different methods for performing the refrigeration process, the majority of refrigeration systems consist of a vapor compression mechanical system. The increase in the problems related to fossil fuels in the world and the lack of technologies in the field of renewable energy in some countries have made it important to improve the optimum operation and performance of refrigeration systems.

In recent years, besides experimental studies, the number of computer simulations has increased and gained importance. In the literature, researchers have also performed CFD analyzes along with thermodynamic models of heating, cooling and ventilation systems [6-8]. Flow, temperature, and pressure analyzes of the solved models were mostly performed in the aforementioned studies. In these studies, an increase in the cooling load and efficiency has been achieved and it has been suggested to improve the sensitive points of the refrigeration systems.

The R290 is a new generation and environmentally friendly refrigerant. Not much CFD work has been done to simulate the thermal performance of R290 in the cold room. In the first part of this article, the thermal performances of R290 and R404A refrigerants in the same vapor compression refrigeration cycle are investigated. In the second part, the time required for the cold room to reach 0 °C from the ambient temperature was determined and CFD analysis was carried out in the light of these data. The results are presented and explained with graphs.

### Materials and methods

Experimental set-up is presented in fig. 1. with schematic picture. The basic elements of the refrigeration system are a hermetic compressor, an evaporator, a condenser, an expansion valve. When both refrigerants were charged to the compressor, they circulated in the system with the same type of oil (polyester). The fans of the evaporator and condenser work with the inverter. The presence of an inverter in the fans contributed to the precise adjustment of the evaporator and condenser temperatures. In this study, the following methods were used while adjusting the evaporator temperatures. A resistor connected to the dimmer was used, adjustment were made by turning the screw of the expansion valve and also the inverter of the evaporator fan was used. In addition, the condenser temperature was adjusted to the determined degree with the inverter of the fan in the

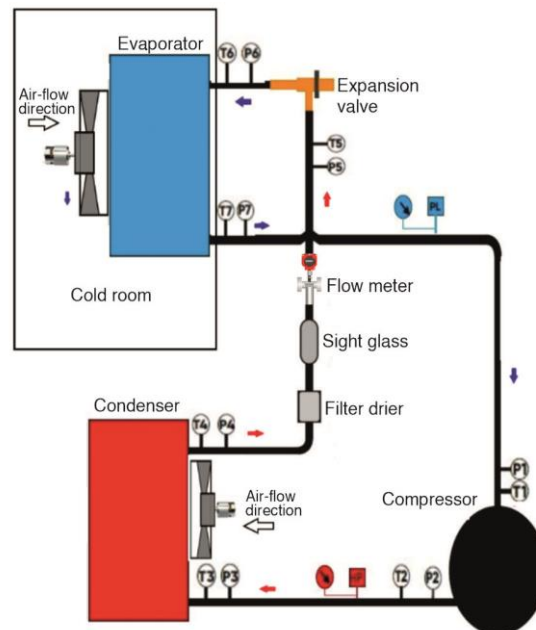


**Figure 1. Schematic of experimental vapor compression refrigeration system**

condenser. In addition, there is a flow meter, a filter drier, a sight glass, and a vacuum pump in the system. Vacuum pump was used during refrigerant exchange. The heat load was given to the cold room through an electrical resistor. The voltage of the electric current passing through the resistor was adjusted with a dimmer.

All sensors connected to the system and their measurement points are given in fig. 1. These sensors are in direct contact with the refrigerant gas circulating in the copper pipes. There are six pressure and temperature sensors at the inlet and outlet of the basic elements in the system. The flow rate of the refrigerants can be detected instantaneously by means of a flow meter. The power consumption of the compressor was recorded with the Wattmeter in the system. All the data taken from the test device were instantly transferred to the computer through the datalogger and plc system. The technical specifications of the measuring instruments of the system are presented in tab. 1.

**Table 1. Details of measurement instruments**

Instrument	Brand	Accuracy
Pressure sensors	DANFOSS	$\pm 0.3\%$
Temperature sensors	REISSMANN	$\pm 0.5\text{ }^\circ\text{C}$
Flow meter	TEKSENS	$\pm 1\%$
Wattmeter	ENTES	$\pm 1\%$

The flow chart of this study is given in fig. 2. in detail. Pictures of pressure and temperature sensors, expansion valve, flow meter, vacuum pump, and compressor used in the test device can be seen in this figure. The experimental setup was designed to comply with the autonomous working principle. Programmable logic controller (PLC) screen makes it possible to control all devices in the system and to monitor data instantly. It has become easier to examine the measured data with PLC automation and to use these data in thermodynamic analysis.

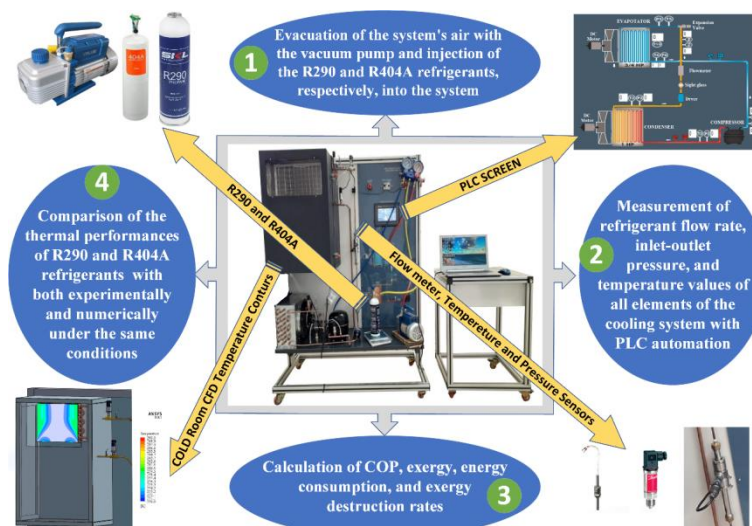


**Figure 2. Flow chart of this study**

Table 2 includes operational parameters used in this study. Evaporator temperatures increasing from  $-5\text{ }^\circ\text{C}$  to  $5\text{ }^\circ\text{C}$  at condenser temperatures extending from  $25\text{ }^\circ\text{C}$  to  $35\text{ }^\circ\text{C}$  were utilized at 3000 rpm compressor rotational speed.

**Table 2. Test conditions**

Operational conditions	R290	R404A
Evaporator temperatures [°C]	-5, 0, 5	
Condenser temperatures [°C]	25, 30, 35	
Compressor rotational speed [rpm]	3000	

The difference in enthalpy values at the inlet and outlet of the evaporator is the basic principle of the cooling capacity calculation. Enthalpy values were gotten using pressure and temperature measurements' data with REFPROP software [9]. The  $\dot{Q}_{\text{evap}}$  [kW] can be determined:

$$\dot{Q}_{\text{evap}} = \dot{m}_{\text{measured}} (h_{\text{evap,o}} - h_{\text{evap,i}}) \quad (1)$$

where  $\dot{m}$  [kgs<sup>-1</sup>] is the mass-flow rate [10]. In a vapor compression refrigeration system, dividing the cooling capacity by the measured compressor power consumption ( $\dot{W}_{\text{comp}}$ ) allows the COP to be calculated. The COP is then calculated:

$$COP = \frac{\dot{Q}_{\text{evap}}}{\dot{W}_{\text{comp}}} \quad (2)$$

Exergy of any point in the system is defined:

$$e_p = (h_p - h_0) - T_0 (s_p - s_0) \quad (3)$$

Flow exergy of any point in the system can be expressed:

$$\dot{E}_p = \dot{m}_{\text{measured}} e_p \quad (4)$$

Exergy destruction in the compressor can be determined:

$$\dot{E}_{\text{dest,comp}} = \dot{E}_{\text{i,comp}} - \dot{E}_{\text{o,comp}} + \dot{W}_{\text{comp}} \quad (5)$$

Second law efficiency of the compressor is defined:

$$\eta_{\text{II,comp}} = \frac{\dot{E}_{\text{o,comp}} - \dot{E}_{\text{i,comp}}}{\dot{W}_{\text{comp}}} \quad (6)$$

Exergy destruction in the evaporator is calculated:

$$\dot{E}_{\text{dest,evap}} = \dot{E}_{\text{i,evap}} - \dot{E}_{\text{o,evap}} - \left( \frac{T_0}{T_L} - 1 \right) \dot{Q}_{\text{evap}} \quad (7)$$

Second law efficiency of the evaporator is detected:

$$\eta_{\text{II,evap}} = \frac{\dot{E}_{Q,\text{evap}}}{\dot{E}_{\text{i,evap}} - \dot{E}_{\text{o,evap}}} \quad (8)$$

where exergy transferred with heat in the evaporator  $\dot{E}_{Q,\text{evap}}$  is found [11]:

$$\dot{E}_{Q,\text{evap}} = \left( \frac{T_0}{T_L} - 1 \right) \dot{Q}_{\text{evap}} \quad (9)$$

Exergy destruction in the condenser can be defined:

$$\dot{E}_{\text{dest,c}} = \dot{E}_{\text{i,c}} - \dot{E}_{\text{o,c}} - \left( 1 - \frac{T_0}{T_H} \right) \dot{Q}_c \quad (10)$$

Second law efficiency of the condenser is expressed:

$$\eta_{II,c} = \frac{\dot{E}_{Q,c}}{\dot{E}_{i,c} - \dot{E}_{o,c}} = 0 \quad (11)$$

where exergy transferred with heat in the condenser  $\dot{E}_{Q,c}$  is equal to zero and can be formulated:

$$\dot{E}_{Q,c} = \left(1 - \frac{T_0}{T_H}\right) \dot{Q}_c = 0 \quad (12)$$

because the reservoir temperature of the condenser and the ambient temperature are equal to each other as follows:

$$T_H = T_0 \quad (13)$$

Exergy destruction in the expansion valve can be calculated:

$$\dot{E}_{dest,ev} = \dot{E}_{i,ev} - \dot{E}_{o,ev} \quad (14)$$

### Uncertainty analysis

Error analysis is of great importance both in the interpretation of the results obtained from the experimental study and in the determination of the appropriate measurement method and tool [12]. In this study, the uncertainty that may be encountered in the measurements of values such as temperature, pressure, flow and power are given in the tab. 3. The uncertainty values specified in tab. 3 were determined according to the sensor flaw, installation error, data transfer error, and other environmental errors.

**Table 3. Errors and uncertainty values in measurement instruments**

Measurement parameter	Error types	Uncertainty value
Temperature	Sensor flaw	±3% [°C]
	Installation error	
	Data transfer error	
	Other environmental errors	
Flow rate	Sensor flaw	±0.2% [gs <sup>-1</sup> ]
	Installation error	
	Data transfer error	
	Other environmental errors	
Pressure	Sensor flaw	±1% [bar]
	Installation error	
	Data transfer error	
	Other environmental errors	
Power consumption	Compressor vibration	±0.4% [W]
	Sensor flaw	
	Installation error	
	Data transfer error	

In measuring the value of a parameter, the total error calculation can be made with eq. (15), taking into account the errors that occur due to fixed errors, random errors and manufacturing errors. In the equation,  $W_R$  is the total uncertainty value,  $R$  is the measured parameter,  $x_1, x_2, \dots, x_n$  are the uncertainties resulting from the total measurement errors in the experimental conditions, and  $w_1, w_2, \dots, w_n$  are the error rates related to the independent variable [13].

$$W_R = \left[ \left( \frac{\delta R}{\delta x_1} w_1 \right)^2 + \left( \frac{\delta R}{\delta x_2} w_2 \right)^2 + \dots + \left( \frac{\delta R}{\delta x_n} w_n \right)^2 \right]^{1/2} \times 100 \quad (15)$$

In this study, the uncertainties in the measurement parameters and the calculation procedure were investigated. Errors of pressure, temperature, flow rate and power consumption measurements and uncertainty values of these parameters are given in tab. 3.

### Numerical solution geometry and mesh model

In fig. 3, a 3-D model of the cooling chamber is given to be used for CFD analysis. A mesh model was created for the numerical solution with multizone. The model's geometry was divided into two parts, and a numerical analysis mesh was performed for a single part with symmetry. The element sizes used in the mesh sensitivity study were 3.5 mm, 3 mm, and 2.3 mm. A similar tendency was seen in the CFD analysis for all three mesh models.

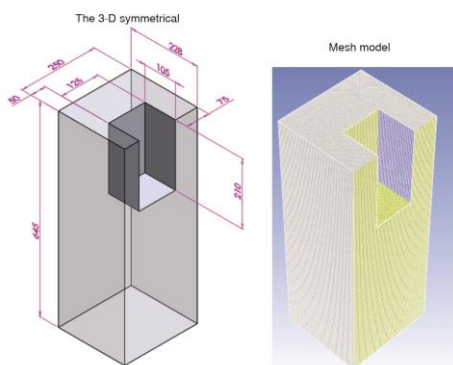


**Figure 3. The 3-D symmetrical model of cooling room and solution mesh model**

Three different mesh configurations presented in tab. 4 were obtained for the R290 refrigerant. The most suitable network model for the experimental results was determined as Model 3. The network structure of this model is shown in fig. 3. As shown in fig. 3, the network structure model is given for the symmetrically separated half region of the cold room. Figure 4 shows the network independence results of the models made for numerical analysis. All of these models have similar trends, as seen in fig. 4. It is seen that the results of all models created by numerical analysis are compatible with the experimental results. Model 3, which is closest to the experimental data and has the fewer error (0.7%), was chosen among the three models.

**Table 4. Statistics of the solution mesh**

Model	Element number	Maximum mesh size [mm]	Minimum mesh size [mm]	Magnification rate	Maximum skew	Minimum average quality	Boundary-layer number	Boundary-layer magnification rate
1	815863	3.5	0.12	1.1	0.50	0.64	12	1.05
2	1646641	3	0.12	1.1	0.51	0.65	12	1.05
3	2931248	2.3	0.12	1.1	0.51	0.66	12	1.05

Turbulence solver  $k$ - $\varepsilon$  equations used in the numerical analysis are as follows [14]:

$$\frac{\partial}{\partial t}(\rho k) + \frac{\partial}{\partial x_j}(\rho k u_j) = \frac{\partial}{\partial x_j} \left[ \left( \mu + \frac{\mu_t}{\sigma_k} \right) \frac{\partial k}{\partial x_j} \right] + G_k + G_b - \rho \varepsilon - Y_M + S_k \quad (16)$$

$$\frac{\partial}{\partial t}(\rho \varepsilon) + \frac{\partial}{\partial x_j}(\rho \varepsilon u_j) = \frac{\partial}{\partial x_j} \left[ \left( \mu + \frac{\mu_t}{\sigma_\varepsilon} \right) \frac{\partial \varepsilon}{\partial x_j} \right] + \rho C_1 S_\varepsilon - \rho C_2 \frac{\varepsilon^2}{k + \sqrt{\nu \varepsilon}} + C_{1\varepsilon} \frac{\varepsilon}{k} C_{3\varepsilon} G_b + S_\varepsilon \quad (17)$$

$$C_1 = \max \left[ 0.43, \frac{\eta}{\eta + 5} \right], \rightarrow \eta = S \frac{k}{\varepsilon}, \rightarrow S = \sqrt{2 S_{ij} S_{ij}} \quad (18)$$

$$\text{Pr}_{\text{energy}} = \text{Pr}_{\text{wall}} = 0.85, C_2 = 1.9, S_k = 1.0, S_\varepsilon = 1.2 \quad (19)$$

Simple numerical algorithm was used for pressure-based equations developed by Patankar and Spalding [15]. Mass, momentum, and energy equations were repetitively solved using numerical methods for respective boundary conditions until related variables (velocity, temperature, pressure, and heat transfer in the wall) reached convergence [15].

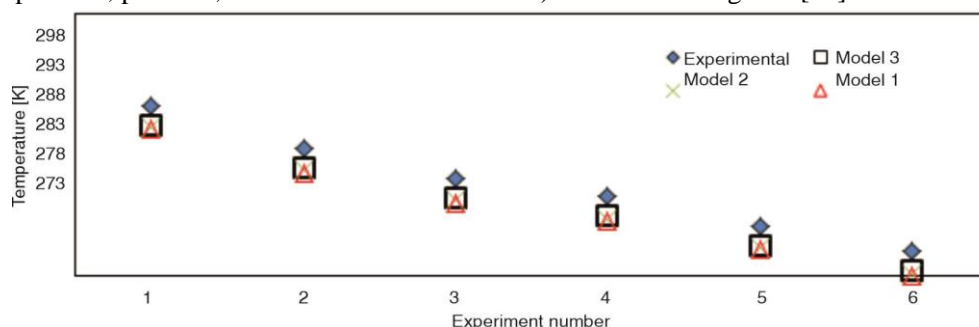


Figure 4. Independence from the solution mesh

Reynolds number was calculated from eq. (20) and the turbulence density,  $I$ , was calculated from eq. (21) and these equations are defined:

$$Re = \frac{\rho \mathcal{Q}_s D}{\mu} \quad (20)$$

$$I = 0.16(Re)^{-1/8} \quad (21)$$

#### Initial and boundary conditions

The most critical term in CFD analysis represents the numerical range in which the numerical analysis model will solve the boundary condition term. This term is expressed as initial and boundary conditions. It is aimed to provide a more straightforward solution to the experimental conditions.

- Air flow is 3D.
- Inlet temperature is constant.
- Air distribution is the same everywhere in the entrance of heat exchanger.
- The walls of the cold room are completely insulated.
- The ratio of turbulence and viscosity was taken as 10.
- Turbulence density,  $I$ , was calculated as 5% from the eq. (21).
- The outlet pressure is taken as zero ( $P = 0$  Pa).
- Air was accepted as an ideal gas.
- The analysis was performed as steady-state for certain temperature intervals.

The analyses used the 0.4 value for the momentum solution control criterion, 0.3 value for turbulence solution control criterion, and default values for other control criteria. The numerical solution lasted until the convergence criteria reached  $10^{-11}$  for the energy equation and  $10^{-6}$  for velocity, continuity, turbulence dissipation, and kinetic energy. The same convergence criteria were taken in lots of the studies in the literature [16-20].

#### Results and discussion

The results of this experimental and numerical study analyzing the thermodynamic performances of two different refrigerants in the same refrigeration cycle are presented with the next figures.

Figure 5 depicts that an increment in the evaporator temperature results with a rise in  $\dot{Q}_{\text{evap}}$ . However, increase in the condenser temperature causes a reduction in the cooling capacity. For instance, cooling capacity values of R290 refrigerant at 0 °C evaporator temperature were 1357.8, 1255.3, and 1135.3 W for 25 °C, 30 °C, and 35 °C condenser temperatures, respectively. In general,  $\dot{Q}_{\text{evap}}$  of R290 showed greater values than R404A. An average 9.38% increase in cooling capacity was observed with R290 refrigerant in comparison with R404A. Under these operational conditions, the highest cooling capacity in the system corresponding to 25 °C condenser and 5 °C evaporator temperatures were 1637 W using R290 and 1574 W for R404A. Figure 5 also shows the change of compressor power consumption at different operational conditions. Increase in evaporator temperature from -5 °C to 5 °C causes an increase in  $\dot{W}_{\text{comp}}$  at a certain condenser temperature. For a specified evaporator temperature, greater power consumption were seen at high condenser temperatures. Generally,  $\dot{W}_{\text{comp}}$  values of R404A were greater than R290 at the same operational conditions in the system. For a specific example, at 25 °C condenser temperature and -5 °C evaporator temperature,  $\dot{W}_{\text{comp}}$  of R290 was 300 W while that of 360 W for R404A. The average of all performed  $\dot{W}_{\text{comp}}$  measurements for R290 was 381.11 W while it was 443.33 W for R404A, and thus 16.33% increase in compressor power consumption was recorded using R404A.

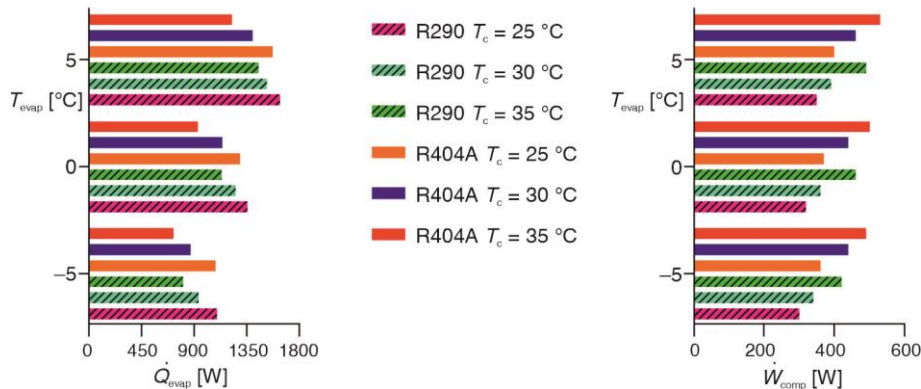


**Figure 5. Change of the cooling capacity and the compressor power consumption at different operational conditions**

Figure 6 shows effect of different operational conditions, namely varying evaporator and condenser temperatures, on COP. The COP of the system increases when the evaporator temperature increases for a certain condenser temperature. Also, COP showed greater values at lower condenser temperatures for a given evaporator temperature. For instance, COP of R404A refrigerant at 0 °C evaporator temperature was 3.5, 2.59, and 1.86 for 25 °C, 30 °C, and 35 °C condenser temperatures, respectively. The COP of the refrigeration system with R290 showed bigger values than R404A in general. Average of all COP calculations in the figure was 3.34 for R290 and 2.63 for R404A and thus an average 27% increase in COP was detected using R290 instead of R404A. Figure 6 also shows fluctuations in COP at  $T_c = 30$  °C and  $T_{\text{evap}} = 0$  °C operational condition using R290 and R404A refrigerants, respectively. In this figure, measurements were recorded after the refrigeration system stabilized at desired condenser and evaporator temperatures. It can be seen from the figure that R404A fluctuated between 2.5 and 2.6 while that of R290 between 3.4 and 3.5.

Figures 7(a) and 7(b) show individual effect of system components at total exergy destruction for  $T_c = 35$  °C and  $T_{\text{evap}} = -5$  °C using both R290 and

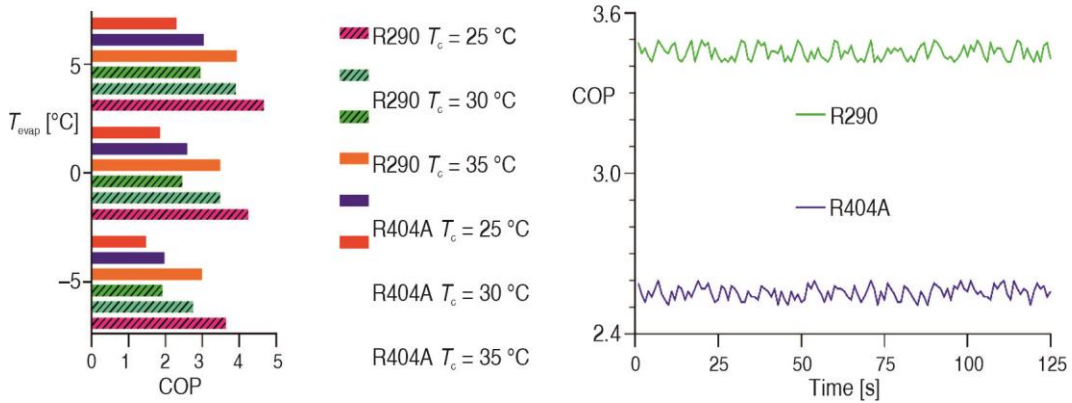


Figure 6. The COP change of the system at varying operational conditions

R404A, respectively. The figure clearly shows that for both R290 and R404A the compressor is the primary cause of total exergy destruction in the system. Considering the exergy destruction rate, the compressor is followed by the evaporator, condenser and expansion valve, respectively. Figure 7(c) indicates Second law efficiency values of refrigeration system components for  $T_c = 35^\circ\text{C}$  and  $T_{\text{evap}} = -5^\circ\text{C}$ . For R290,  $\eta_{II}$  of the compressor was nearly 47.5% while that of evaporator 29%. For R404A,  $\eta_{II}$  of the compressor was around 39% while that of evaporator 26%. There was no recoverable exergy for the condenser and the expansion valve and thus they showed zero  $\eta_{II}$ . Heat sink temperature of the condenser and ambient temperature were selected as equal and thus the condenser presented zero  $\eta_{II}$ .

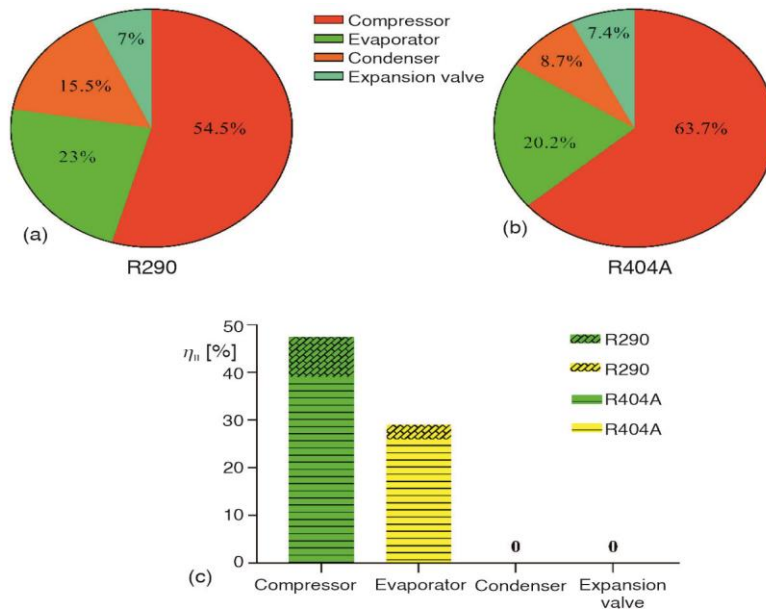


Figure 7. Exergy destruction rates and second law efficiency values of the system components

Figure 8 shows the time it takes for the temperature of the cold room to reach 0 °C from ambient temperature. The data were recorded at  $T_c = 25$  °C and  $T_{\text{evap}} = -5$  °C operational conditions. It can be seen from the figure that R290 cools the room faster and causes a room temperature of 0 °C to be reached more quickly than R404A. The measured time for R290 refrigerant was approximately 480 seconds, compared to 740 seconds for R404A. The values of nine different points presented in this figure were utilized in the CFD analysis.

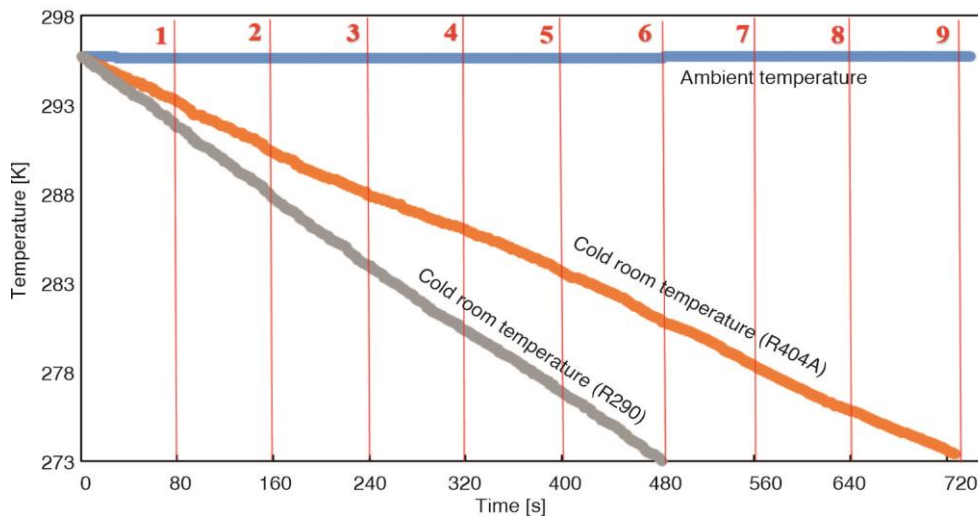


Figure 8. Change of cold room temperature with R404A and R290

The second part of this study was performed using ANSYS FLUENT R18.1. Error analyses of the numerical results were performed using eq. (22). Error rate of all analyses are under 1 % with Kelvin unit:

$$\text{Error}_{\text{Abs}} \% = \left| \frac{T_{\text{num}} - T_{\text{exp}}}{T_{\text{exp}}} \right| \times 100 \quad (22)$$

The CFD results are presented in tab. 5. and in the figs. 9-11. When tab. 5. is investigated, it is understood that R290 refrigerant cools the room with fewer number of experiments compared to R404A. Because of the fact that the cooling room reached 0 °C using R290 before R404A, two more experiments were performed using R404A.

Table 5. The CFD results

Experiment number	R404 experimental evaporator outlet temperature [K]	R404 numerical analysis result [K]	R290 experimental evaporator outlet temperature [K]	R290 numerical analysis result [K]
1	290.6	290.3	288.3	289.1
2	286.2	285.1	283.8	284.7
3	283.1	285.9	280.4	283.1
4	281.2	283.2	276.2	276.9
5	278.2	280.4	273.8	274.1
6	275.6	276.3	270.1	271.1
7	273.9	275.2	268.6	269.2
8	270.1	271.1	–	–
9	269.1	270.1	–	–

Figure 9 shows the air streamlines of the cold room. Since the evaporator is located in the horizontal center of the cold room, it is understood that the air reaches even the farthest and most corner point of the room.

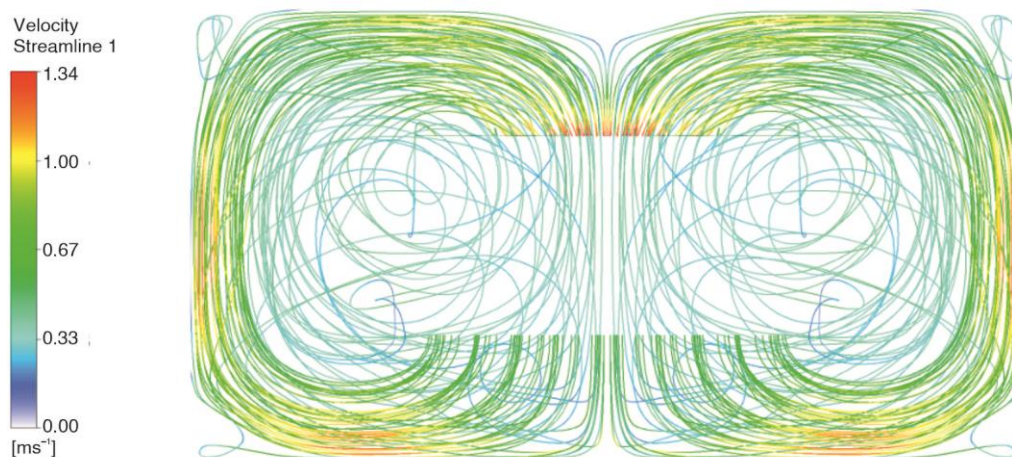


Figure 9. Cold room velocity streamline

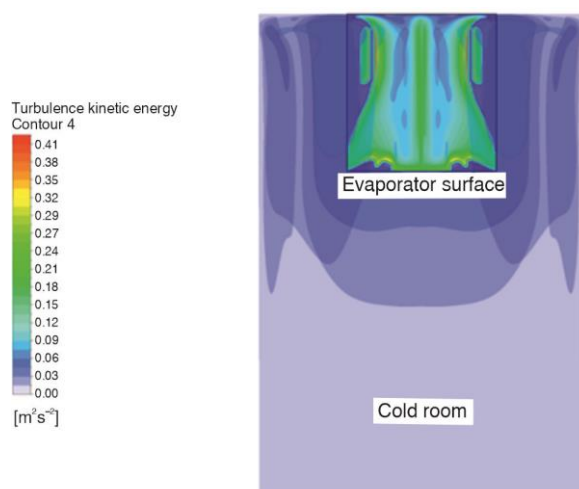


Figure 10. Cold room turbulent kinetic energy contour

11(a)-11(c) are the 2<sup>nd</sup>, 4<sup>th</sup>, and 6<sup>th</sup> analyses for R404A and figs. 11(d)-11(f) for R290, respectively. Here, when the figs. 11(a)-11(c) are examined, the color darkness of the high-temperature regions is seen more intensely. According to the numerical analysis results, R290 gas cools the evaporator surface more, and thus the cold room cools faster.

## Conclusion

In this study, in which the thermal performances of refrigerants are investigated both experimentally and numerically, the performances of R290 refrigerant with a GWP value close to zero and old generation R404A refrigerant are compared. Evaporator temperatures of

The turbulent regions in the cold room are shown in fig. 10. Turbulent regions in the cold room indicate that hot air and cold air mix quickly. In the lower part of the figure, it is seen that this mixture is gradually decreasing. In this case, it is thought that a better mixture will be created if the evaporator is located close to the middle part of the cold room rather than at the top.

Figure 11 shows the temperature distribution in the inlet area of the evaporator in the cold room. According to the 3-D model, the air outlet area is defined as the front surface of the evaporator. Figures

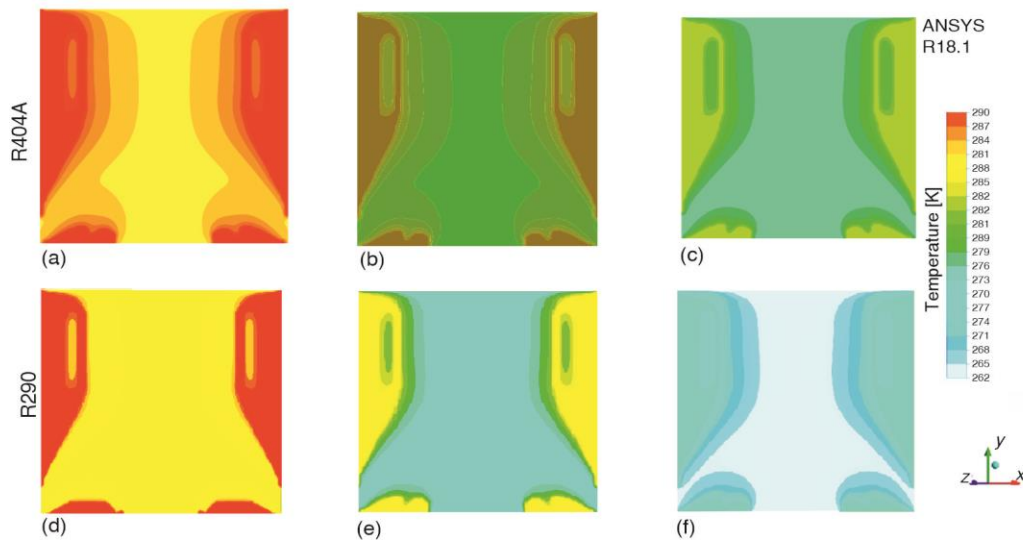


**Figure 11. Cold room evaporator outlet surface temperature contours**

$-5\text{ }^{\circ}\text{C}$ ,  $0\text{ }^{\circ}\text{C}$ ,  $5\text{ }^{\circ}\text{C}$ , and condenser temperatures of  $25\text{ }^{\circ}\text{C}$ ,  $30\text{ }^{\circ}\text{C}$ ,  $35\text{ }^{\circ}\text{C}$  were chosen as operational parameters. The relationship of various operational parameters with COP, cooling capacity, and energy consumption were shown. Also, CFD was performed in the cooling room. The results achieved in this study are summarized as follows.

- The R290 showed higher COP values than R404A in all cases. An average of 27% increase in COP was detected using R290 instead of R404A. The highest COP values in the refrigeration system with R290 and R404A were 4.68 and 3.94, respectively.
- An average 9.38% increment in the cooling capacity was determined with R290 compared to the R404A refrigerant.
- The R404A caused an average 16.33% increase in power consumption compared to R290.
- The time necessary for cold room temperature to arrive from environment temperature to  $0\text{ }^{\circ}\text{C}$  was detected to be 35.1% less than R404A using R290.
- The compressor was the primary source of irreversibility in the system. Evaporator, condenser, and expansion valve followed the compressor in exergy destruction, respectively.
- Solution of the experimental results using numerical analysis with less than 1% error was performed.
- Air streamline contours and turbulent kinetic energy contours of the designed cold room are given. It has been understood that the evaporator should be placed slightly lower than the ceiling in the cold room.
- Numerical analysis temperature simulation results showed that the evaporator surface has a lower evaporator surface temperature with R290 refrigerant than R404A.

As a result of this study, the usability of the new generation R290 refrigerant compared to the old generation R404A refrigerant in the vapor compression refrigeration system has been demonstrated with a thermal approach and CFD analysis results.

### Nomenclature

$\dot{E}$  – flow exergy, [kW]  
 $e$  – exergy, [ $\text{kJkg}^{-1}$ ]

$h$  – enthalpy, [ $\text{kJkg}^{-1}$ ]  
 $\dot{m}$  – mass-flow rate, [ $\text{kgs}^{-1}$ ]

$P$  – pressure, [bar]  
 $\dot{Q}$  – heat transfer rate, [kW]  
 $T$  – temperature, [°C]  
 $\dot{W}$  – compressor power consumption, [kW]

*Greek symbol*

$\eta$  – efficiency

*Subscripts*

c – condenser  
comp – compressor  
dest – destruction  
ev – expansion valve

evap – evaporator  
H – high temperature reservoir  
i – inlet  
L – low temperature reservoir  
p – any point in the system  
o – outlet  
0 – ambient  
II – second law

*Acronyms*

GWP – global warming potential  
ODP – ozone depletion potential  
PLC – programmable logic controller

## Acknowledgement

Authors would like to thank Tokat Gaziosmanpaşa University Scientific Research Foundation for supporting this study with the project number of 2020/122.

## References

- [1] Belman-Flores, J. M., et al., Exergy Assessment of a Refrigeration Plant Using Computational Intelligence Based on Hybrid Learning Methods, *Int. J. Refrig.*, 88 (2018), Apr., pp. 35-44
- [2] Zendejboudi, A., et al., Modeling and Multi-Objective Optimization of an R450A Vapor Compression Refrigeration System, *Int. J. Refrig.*, 100 (2019), Apr., pp. 141-155
- [3] Harby, K., Hydrocarbons and Their Mixtures as Alternatives to Environmental Unfriendly Halogenated Refrigerants: An Updated Overview, *Renew. Sustain. Energy. Rev.*, 73 (2017), C, pp. 1247-1264
- [4] Nair, V., HFO Refrigerants: A Review of Present Status and Future Prospects, *Int. J. Refrig.*, 122 (2021), Feb., pp. 156-170
- [5] Colbourne, D., et al., General Framework for Revising Class A3 Refrigerant Charge Limits – A Discussion, *Int. J. Refrig.*, 117 (2020), Sept., pp. 209-217
- [6] Lu, H., Lu, L., CFD Simulation of Liquid Desiccant Dehumidifier Performance with Smooth and Rough Plates, *Int. J. Refrig.*, 124 (2021), Apr., pp. 1-12
- [7] Chiang, W.-M., et al., Performance Improvement of an Industrial Control Enclosure Cooling System, *Thermal Science*, 26 (2022), 3A, pp. 2043-2052
- [8] Li, X., et al., Critical Heat Flux Analysis of Divertor Cooling Flow Channel in Fusion Reactor with CFD Method, *Thermal Science*, 26 (2022), 2C, pp. 1855-1869
- [9] Lemmon, E. W., et al., Reference Fluid Thermodynamic and Transport Properties Database-Version 8.0. vol. 23. Gaithersburg: Standard Reference Data Program; 2013
- [10] Selimefendigil, F., Oztop, H. F., Exergetic Performance of Vapor-Compression Refrigeration System with TiO<sub>2</sub> Nanoadditive in the Compressor Oil, *Thermal Science*, 25 (2021), 1B, pp. 637-642
- [11] Pektezel, O., Acar, H. I., Energy and Exergy Analysis of Combined Organic Rankine Cycle-Single and Dual Evaporator Vapor Compression Refrigeration Cycle, *Appl. Sci.*, 9 (2019), 23, 5028
- [12] Holman, J. P., *Experimental Methods for Engineers*, 8<sup>th</sup> ed., McGraw-Hill, New York, USA, 2012
- [13] Kline, S., McClintock, F., Describing Uncertainties in Single-Sample Experiments, *Mechanical Engineering*, 75 (1953), Jan., pp. 3-8
- [14] You, Y., et al., A Flexible Hybrid CFD Model for Refrigerant Mal-Distribution Among Minichannels in Parallel Flow Condensers, *Int. J. Refrig.*, 91 (2018), July, pp. 80-88
- [15] Patankar, S. V., Spalding, D. B., *A Calculation Procedure for the Transient and Steady-State Behaviour of Shell-And-Tube Heat Exchangers*, Imperial College of Science and Technology, London, UK, 1972
- [16] Ahmadi, V. E., Erden, H. S., A Parametric CFD Study of Computer Room Air Handling Bypass in Air-Cooled Data Centers, *Appl. Therm. Eng.*, 166 (2020), Feb., 114685
- [17] Das, M., et al., Numerical and Experimental Analysis of Heat and Mass Transfer in the Drying Process of the Solar Drying System, *Eng. Sci. Technol. an Int. J.*, 24 (2021), 1, pp. 236-246
- [18] Alic, E., et al., Design, Manufacturing, Numerical Analysis and Environmental Effects of Single-Pass Forced Convection Solar Air Collector, *J. Clean. Prod.*, 311 (2021), Aug., 127518

- [19] Das, M., *et al.*, Detailed Analysis of Mass Transfer in Solar Food Dryer with Different Methods, *Int. Commun. Heat Mass Transf.*, 128 (2021), Nov., 105600
- [20] Aydin, A., *et al.*, Optimization and CFD Analysis of a Shell-And-Tube Heat Exchanger with a Multi Segmental Baffle, *Thermal Science*, 26 (2022), 1A, pp. 1-12